Delineating fluid flow paths beneath the Mound Springs, Great Artesian Basin, using magnetotellurics.

University of Adelaide
Geophysics Honours 2010
James Wilson 1162166

Supervisor: Graham Heinson

Contents

Delineating fluid flow paths beneath the Mound Springs, Great Artesian Basin, using magnetotellurics.

Abstract:

There is a lack of understanding about the mechanisms that control characteristics about the mound springs of the Great Artesian Basin (GAB). There is question about the origins of water that feed the springs. There is the possibility of local infiltration providing a shallow source of fluid and a deeper source on a more regional scale. How the springs are structurally controlled by faults and to what extent local recharge feeds back into the springs are all areas of active research. Beresford Spring is a mound spring located in the southwest of the Great Artesian Basin, approximately 50 km west of Lake Eyre South. It is one of over 600 springs that are spread throughout the GAB of which over 40% are no longer active. The geology is poorly constrained due to the lack of significant outcrop as a result high weathering and sedimentary cover. Geophysical techniques are cheap and effective method of looking through this cover. This study involves the use of magnetotellurics (MT), which is a low impact, cheap technique that can be used to image the subsurface resistivity without causing significant damage to the local ecosystem, unlike seismic surveys for example. It is used to measure the resistivity of the Earth at varying depths and resolutions. The survey consisted of a north-south line and an east-west line that were used to generate 2D inversion models with the goal of being able to differentiate between the spring and the surrounding confining beds and to delineate fluid flow paths feeding the springs. The results show that Beresford Spring is marked by a resistive high, a 10 fold increase compared to its immediate surroundings. Phase tensor plots reveal that at depth, the preferential direction of electrical current flow is in a northeast-southwest orientation over the entire Beresford region. At shallow depths, the region becomes homogeneous and loses any preferential orientation in conductivity. Beresford Spring maintains its northeast-southwest tensor which is an indication of the fluid pathways that feed the spring.

Introduction:

The Great Artesian Basin is the largest and deepest artesian basin of its kind in the world (Torgersen *et al.* 1992). It extends across Queensland, New South Wales, The Northern Territory and South Australia, covering over 1.7 million square kilometres (Figure 1). It is estimated that the basin contains approximately 8700 million mega litres of water (NRM 2006). Mound springs are domed shaped sedimentary accumulations that are fed by rising groundwater from the Great Artesian Basin. They are important because the presence of a stable year round supply of water has allowed for the development of extensive ecosystems across the hundreds springs that occur across the Great Artesian Basin. This biodiversity is threatened by the drawdown of the springs, which only exist due to the stable water supply. Without the presence of the springs, the local environment would be largely inhospitable similar to elsewhere within the outback, potentially destroying the local flora and fauna that has grown dependent on the springs to survive.

There is a significant lack of knowledge regarding the mound springs within the Great Artesian Basin. It is unknown to what extent the springs are fed by shallow or deep sourced fluids. It is possible that there is an element of local recharge that occurs, via local rainfall or the spring feeding back into itself that contributes to the spring discharge, representing shallowly sourced fluids. Deeper sourced fluids would be from the basin aquifers on a more regional scale, with water infiltrating from the Great Dividing Range and the western margin of the basin. The fluid pathways that feed the springs are controlled structurally by faults, yet the springs only occur at certain points along these faults. The extent of these pathways is in question, it is likely that

they are localised directly below the springs which would make them difficult to resolve on large scale surveys.

The purpose of this study is to fill the knowledge gaps that exist around the mound springs. Since the geology at Beresford is largely undercover, geophysical techniques are an effective and cheap method of circumventing this lack of outcrop. Magnetotellurics allows us to fill this gap in knowledge by allowing for the differentiation between the springs and the surrounding landscape and allowing for the delineation of the fluid pathways that feed the springs.

Resistivity variations that occur within the study site are predominantly controlled by the presence of fluids. The electrical properties of soils and rocks are determined by water content, the mineralogy, clay content, salt content, porosity, and the presence of metallic minerals (Kress & Teeple 2003). Typically the resistivity of the water has a larger effect on the bulk resistivity than the soil or rock type (Kress & Teeple 2003). The aquifer and spring will be more resistive due to flow of relatively freshwater. The aquitard surrounding the spring will be more conductive due to salty water containing ions trapped within surrounding clay rich rocks.

Hydrogeology of the Great Artesian Basin:

The Great Artesian Basin formed over millions of years during the Lower Cretaceous, Jurassic and Triassic periods (Torgersen *et al.* 1992), and consists of alternating layers of permeable sandstones and impermeable silt and mudstones. The sandstones were deposited by rivers and streams, which were subsequently overlain by silt and mudstones, which were deposited by lakes and floodplains (NRM 2006). The Great Artesian Basin is comprised of three smaller sub-basins, known as the Carpentaria, the Eromanga and the Sturt. The site of interest in this study, Beresford Spring, is located within the Eromanga Basin.

There are over 5000 active bores (Love & Herczeg 2007) within the GAB and when first drilled, many flowed at rates greater than 10 megalitres per day (ML/d), presently the majority flow between 0.01-6 ML/d. At its peak in 1915, total outflow from the basin reached just over 2000 ML/d but since then has declined to approximately 1500 ML/d (NRM 2006). Due to extensive use in the previous century, about one third of all artesian bores which flowed naturally now require pumps to bring water to the surface (NRM 2006). This is because under regulation has resulted in over extraction causing local depressions in hydrostatic pressure.

Recharge within the basin occurs primarily along the eastern margin, along the Great Dividing Range where the permeable sandstone aquifers are exposed at the surface in moist tropical conditions. To a lesser extent, recharge also occurs along the western margin, towards Central Australia. Prior to development within the basin, it was estimated that 1040 ML flowed daily into the Great Artesian Basin (NRM 2006). Water within the basin has been analysed by Carbon-14 and Chlorine-36 dating, which gives ages of several thousand years in the north near zones of recharge and up to two million years in the southwest along the farthest extents of the basin (Mudd 2000). It has been suggested that the GAB system is not in equilibrium, the main driver is palaeo recharge which is induced by climate variability (Love & Herczeg 2007).

Water within the aquifer flows out naturally through a series of artesian springs along faults or other naturally occurring pathways that allow fluid flow (Figure 2), i.e. they are structurally controlled (Williams & Holmes 1978). The extent at which the water will flow out of the springs is dependent on the hydrostatic pressure. An aquifer with a large hydrostatic pressure will allow water from an artesian well to rise higher than an aquifer with a lower pressure. Over-extraction of water from the basin (e.g. bores) can result in localised drawdown around the source of extraction and a lower hydrostatic pressure, which will have a negative impact on the rate of

flow from the artesian springs. In some cases if the use of water is not correctly monitored, the pressure can drop to substantially low enough levels to stop water flowing from springs altogether.

Mound Springs

The site of the survey (Figure 1), Beresford Spring, is a type of artesian spring known as a mound spring. They are so named due to the tendency to exhibit mound or hummock shapes, which is a result of the accretion of sediments from waters flowing from the aquifer around the spring outlets eventually building up to form a mound (Williams & Holmes 1978).

These accreted sediments are typically limestone, consisting of tufa or calcrete, or carbonate cemented sandstones (Keppel 2009). The deposition of these carbonates is limited to areas of permanent surface water. The mounds are predominantly built of tufa and modern tufa precipitation is restricted to the tail environment where the water pools into swamps or shallow graded streams (Keppel 2009). It has been suggested (Keppel 2009) that compositional variations in the springs may be due to changes in the point source of CO_2. The accretions form a conical shape often with a crater filled with a pool of water at the top. Water flowing from this pool will flow over the mound and form a tail that begins to fan out, feeding into a small delta (Box *et al.* 2008).

The presence of this stable, year-round supply of water has allowed for the development of extensive ecosystems surrounding active springs that would not otherwise exist (ALNRMB 2008). These ecosystems are threatened by decreased hydrostatic pressures, which dictate how much water flows from the springs. Over 40% of all springs are now inactive due to over-extraction from bores throughout the GAB (Love *et al.* 2000). Eventually the mounds can grow to a large enough size that the rising water no longer has the pressure to reach the surface of the mound and the spring will become extinct. They will then often relocate to a less resistive position and begin forming again. The mounds are typically around 8 meters in height and 30 meters in diameter. Hamilton Hill Spring, currently extinct, reached a height of 40 meters, which suggests that the hydrostatic pressure within the Great Artesian Basin has been higher in the past then today's level (Habermehl 1980). The springs were also responsible for early European expansion north through Central Australia as they provided potable water for drinking and eventually a source of water for steam locomotives, most notably the old Ghan train.

Beresford Spring / Local Geology

Beresford Spring is located in the south-western portion of the Great Artesian Basin approximately 50 km west of Lake Eyre South. The aquifer largely consists of permeable sandstones that are bounded by impermeable silts and mudstones (NRM 2006). Figure 4 is a geological cross-section of the region surrounding Beresford Spring (Love & Herczeg 2007). The geology is not very well constrained due to the lack of significant outcrop. The geology dips to the south east at approximately 30 degrees. The region is comprised of the Oodnadatta Formation, the Bulldog Shale, the Cadna-owie Formation, the Algebuckna Formation and Adelaideian Sediments (NRM 2006).

There is a series of poorly constrained faults that occur across the cross-section and it is thought that some of these faults are responsible for the artesian springs by providing fluid pathways. Figure 3 is a schematic representation of a mound spring which shows how a structure, such as a fault, can control fluid flow by breaking through the aquitard unit. Beresford itself is fed by water from the Cadna-owie Formation via a fluid pathway through the Bulldog Shale (NRM 2006). The springs occur along these faults at points, rather then there being continuous seepage across the fault. This indicates that there must be some form of

preferential flow path along the fault that results in some locations being more favourable for the formation of springs then others.

At the survey site there are two, reasonably large extinct mounds that lie to either side of springs, Beresford and Warburton. For several hundred meters, the surface surrounding Beresford consists of salt scalded mudflats and a depression which collects local rainfall. This is part of a larger drainage network that eventually feeds into Lake Eyre South.

Data available is from Warburton spring, which occurs at the Beresford site in close proximity to Beresford Spring. The spring discharges at a rate of 185 L/m at a temperature of 23.8˚C. The water has a Total Dissolved Salt (TDS) content has 4.276 g/L and a pH of 7.03, an EC value of 6.578 mS/cm C and 0.2% Dissolved Oxygen (DO). Warburton spring has high partial pressures of CO_2 and high levels of SO_4 and Na^+(Keppel 2009). The data was collected on the 16th of June 2009.

It is unknown as to what extent water flowing from the springs is from shallow aquifers or from deeper, mantle derived sources. It would be possible to determine this by looking at He^3/He^4 ratios. The majority of data collected indicates that He4 concentrations are far in excess of in situ production, in some cases a tenfold increase. Rn^{222} data indicates that He production throughout the basin remains relatively consistent (Torgersen 1980) which fails to explain the high He^4 levels. These observations suggest that there is an input of He^4 from outside the aquifer system (Torgersen & Clarke 1985).

Magnetotelluric Method:

Magnetotellurics is an electromagnetic, geophysical method that uses naturally occurring geomagnetic variations as a source of electromagnetic induction within the Earth. Mt is a technique that allows for the imaging of the subsurface resistivity without the need for expensive and environmentally destructive methods such as seismic. It can be used to measure the subsurface conductivity of the Earth at varying depths and resolutions. Low frequency variations are used to measure deeper depths at lower resolutions. High frequency variations are used to measure shallower depths at higher resolutions (Simpson & Bahr 2005).

Induction

The source field for MT is the Earth's magnetic field, which varies as a function of time. A time varying magnetic field will induce a current within a conductor, which in this case is the Earth depicted in Figure 5 (Simpson & Bahr 2005). The bandwidth of frequencies used for MT is approximately 10^{-4}Hz to 10^4Hz (10^4s to 10^{-4}s). There is a dead band that is located within the range of 10^1Hz to10^{-1}Hz (0.1s to 10s), this is due to very few natural sources of variation at these frequencies. Electrical storms provide the source field for induction at frequencies >10^{-1}Hz while magnetic storms provide for <10^{-1}Hz(Simpson & Bahr 2005). Lightning strikes cause radially expanding magnetic fields which propagate through the atmosphere with almost no attenuation. At a distance sufficiently far enough from the strike, this will appear as a uniform plane-wave source. The high global frequency of thunderstorms, specifically around the equator makes lightning a reliable and consistent source of EM induction (Figure 6). Magnetic storms and pulsations are caused by the resonation of electrons within the ionosphere. They occur over a very wide area and also behave like a plane-wave source at distance. Magnetic storms are a result of solar activity disrupting the magnetic field which acts as a uniform inducing field at most latitudes (Simpson & Bahr 2005). Maxwell's equations are used to describe electromagnetic induction within a conductor, which are listed below(Simpson & Bahr 2005).

$$1)\ \nabla * E = -\frac{\partial B}{\partial t} \qquad 2)\ \nabla * B = \mu_0 \sigma E \qquad 3)\ \nabla * B = 0 \qquad 4)\ \nabla * E = \frac{n_t}{\varepsilon}$$

1. Maxwell-Faraday Law of Induction (where E is the electric field, B is the magnetic field and t is time).
2. Ampere's Circuital Law (where B is the magnetic field, μ_o is the permeability of free space, σ is permittivity of free space and E is the electric field).
3. Gauss's Law for Magnetism (Where B is the magnetic field).
4. Gauss's Law (where E is the electric field, n_t is the total charge density and ε is the permittivity of free space.

Electric and magnetic fields obey diffusion equations within a conducting material. These are determined by taking the curl (∇) of the first two of Maxwell's equations, and provide information about the conductivity of the Earth.

$$1)\ \nabla^2 E = \mu_0 \sigma \frac{\partial E}{\partial t} \qquad 2)\ \nabla^2 B = \mu_0 \sigma \frac{\partial B}{\partial t}$$

1. Where E is the electric field, μ_o is the permeability of free space, σ is permittivity of free space and t is time.
2. Where B is the magnetic field, μ_o is the permeability of free space, σ is permittivity of free space and t is time.

Impedance is a measurement of the ratio of the orthogonal components of the electric and magnetic fields, relating the incident magnetic and induced electric fields within a conductor (Simpson & Bahr 2005).

$$\begin{pmatrix} Z_{xx} & Z_{xy} \\ Z_{yx} & Z_{yy} \end{pmatrix} \begin{pmatrix} B_x \\ B_y \end{pmatrix} = \begin{pmatrix} E_x \\ E_y \end{pmatrix}$$

Where Z represents the different components of the impedance, E_x and E_y represent the xy components of the electric field while B_x and B_y represent the xy components of the magnetic field. Impedance is used to determine the apparent resistivity of the conductor and phase shift between the electric and magnetic fields. At any measured period, the impedance tensor will be the volumetric average of the subsurface as defined by the skin depth. Unless the subsurface is a uniform half-space, the absolute resistivity cannot be directly calculated, so we instead calculate the apparent resistivity (Simpson & Bahr 2005). This is defined as the average resistivity of an equivalent uniform half-space and is calculated with the components of Z using the following equation:

$$\rho_{a=\frac{1}{\mu\omega}[Z]^2}$$

Where Z is the impedance, μ is the permeability of free space and ω is equal to $2\pi f$, where f is the frequency(Simpson & Bahr 2005). The impedance tensor also contains information about phase Φ. The phase is a measurement of the lag between the inducing magnetic field and the induced electric field. It is determined using the following equation:

$$\phi = \arctan(Z)$$

The behaviour of the electric and magnetic fields and subsequently the impedance tensor depends on the dimensionality of the Earth. The Earth can be either 1D, 2D or 3D. A 1D model is the simplest model and consists of a horizontal layering where conductivity changes in only the vertical (Z) direction and not the horizontal (X and Y). A 2D model consists of a horizontal layering where conductivity changes in the vertical (Z) direction and one horizontal (X or Y) direction. A 3D model consists of conductivity changes in the vertical (Z) direction and both horizontal (X and Y) directions. There are two different modes that the MT tensor can decompose to transverse electric (TE) or transverse magnetic (TM). TE mode describes the process by which the electric field is measured parallel to strike while TM mode is describes measuring the magnetic field parallel to strike (Simpson & Bahr 2005). These modes only exist

for 2D subsurface where electric and magnetic fields are measured parallel and perpendicular to strike.

Penetration Depth

Long period signals penetrate deeper within the Earth than short period signals. The depth of penetration of the magnetic field variations depend on period length and the conductivity of the subsurface, this is known as the skin depth. The skin depth is given by the following equation:

$$\delta = \sqrt{\frac{2}{\mu_0 \sigma \omega}}$$

Where μ_0 is the free air permeability ($\mu_0 = 4\pi \times 10^{-7}$ NA^{-2}), σ is the conductivity in S/m and ω is equal to $2\pi f$, where f is the frequency (Simpson & Bahr 2005).Magnetic permeability does not typically vary substantially within the Earth. This allows us to re-write the equation.

$$\delta = 500\sqrt{T\varrho}$$

Where T is the period in seconds and ϱ is the apparent resistivity.

Depending on the frequency and conductivity of the medium and the period, the energy can penetrate from tens of meters to thousands of kilometres. The skin effect defines the depth at which the magnetic field signal has decreased to e^{-1} of its original amplitude at the surface. It is controlled by a process by which currents tend to distribute themselves within a conductor such that the current density near the surface is greater than that closer to the core. This causes the resistance of the conductor to increase with the frequency of the current, hence why long period signals penetrate deeper then short period signals.

Method:

Instrumentation

Instrumentation consisted of 4 component MT systems that measured E_x, E_y, B_x and B_y fields (Figure 6). The electric fields E_x and E_y were measured using 3 inch diameter, $CuSO_4$ half cell reference electrodes (Tinker & Rasor, Model 3A “Fat Boy”). The magnetic fields B_x and B_y at 500Hz were measured using induction coil magnetometers (Laboratory of Electromagnetic Innovations, Model Lemi 120). For the 10Hz long period survey, in place of the LEMI magnetometers, Bartington Sensors (Model Mag-03MS7000) were used to measure the magnetic fields B_x and B_y. The Bartington Sensors can measure the magnetic field in three orientations. Only 2 long period sites were collected due to inclement weather. The instruments were all connected to a data logger (Earth Data Model PR6-24 Portable Field Recorder) which has a waterproof enclosure and removable hard disk for ease of data collection.

Data Collection

The default recording axis for the electric and magnetic fields was in a north-south and east-west orientation. For the electric field, the electrode dipoles were laid out at an average of 50m in the above orientations. This consisted of 3 electrodes, one to the north, one to the east and the other acting as a central point. The electrodes were buried in small holes which were wet using water (to assist with the electrical connection) prior to burying them so only the top was exposed. By measuring the voltages at each electrode and knowing the distances between electrodes, the electric field E can be determined by the following equation:

$$E = V/D$$

Where V is the voltage and D is the distance. Induction coils were used to sample the data at 500Hz for every site to measure the magnetic field and Bartington sensors sampled at 10Hz. They were oriented on a similar north-south and east-west axis, levelled and buried to a depth of 5-10cm. The data logger and battery were placed inside a hard protective case to prevent damage from weather and animals. They were also placed in inconspicuous locations where necessary to deter public interference. At each site a laptop was used to ensure the correct recording parameters were used and to make sure that the electric and magnetic fields were

within acceptable ranges before setting the logger to 500Hz prior to departure. If there was an anomaly in one of the electric or magnetic channels, the electrode or magnetometer would be moved to a different position and the cables checked until an acceptable result was achieved.

Originally, the intent was to perform two large transects of long period data sampled at 10Hz along NW-SE and NE-SW lines at 5km spacing's. A short period survey consisting of two large scale transects of short period data sampled at 500Hz along NW-SE and NE-SW lines at 500m spacing's was collected, also a broadband grid pattern surrounding Beresford Spring sampled at 500Hz at 500m spacing's. However due to poor weather conditions, the field deployment had to be modified. A total of 20 broadband 5 channel MT soundings at a sample rate of 500Hz were acquired as well as two remote sites. 2 long period soundings at a sampling rate of 10Hz were collected using the Bartington Sensors. Data acquisition was performed during winter, from July 11-17th 2010.

Processing

BIRRP (Bounded Influence Remote Reference Processing) is a program that computes magnetotelluric and geomagnetic depth sounding response functions using a bounded influence, remote reference method (Chave & Thomson 2004). It was used to process all sites for this study.

Coherence thresholding is a statistical process that rejects data that does not fall within a pre-defined boundary. A low threshold rejects a smaller proportion of data compared to a high threshold. For the purpose of this study, thresholds ranging from 0.3 to 0.8 were experimented with (Chave & Thomson 2004). The data was processed with a threshold of 0.5, which was deemed to give the best trade off between noise and data quantity.

Remote referencing is a method that is used to remove unwanted noise from survey data. The basic idea is that by measuring the magnetic field simultaneously at two different sites and comparing, the magnetic signal will be the same while the noise will be uncorrelated(Chave & Thomson 2004). This is due to there not being very large spatial differences between the magnetic fields at different sites. Any noise that is contained within the magnetic data will be caused by local variations specific to the measurement location. If we assume that the actual signal at both sites is the same, we can estimate what part is correlated signal and what part is uncorrelated noise. It is then possible to drop the noise, leaving dramatically improved signal quality.

Figure 9.1 and 9.2 show the increase in signal quality that was achieved using coherence thresholds and remote referencing for the site MB10. Figure 9.1 shows apparent resistivity vs. frequency. This plot is of raw data which had not undergone any filtering. Figure 9.2 shows the same plot as 9.1 but is post-processing and has a much better signal to noise ratio. These figures show how significant the improvements in signal quality can be with simple filtering.

Modelling

Magnetotellurics is a volume sounding method. This means that data collected from depths greater than the spacing between stations will be recorded by multiple stations. The process of inversion (using WinGLink) integrates the data collected from multiple stations into a single model point (Rodie & Mackie 2001). This gives a much more reliable and accurate representation as the inverted data has been referenced by more than one source. A smoother model containing reliable structures and constraints is preferable to a less smooth model that contains unrealistic structures and is unconstrained.

Tau is a regularization parameter that is responsible for determining whether model smoothness or model fit is of more importance. Large values of tau create a smoother model, but do so at the expense of data fit. Smaller values produce a much rougher model which is more truthful to the data fit. The root mean squared (RMS) error is a measure of the difference between the modelled data and the station data for all parameters (apparent resistivity and phase) involved in the inversion process. A high RMS tells us that there is a large difference or error, between the model and the un-inverted station data. A low RMS tells us that the model is accurate and truthful to the station data. Although it is possible to decrease the RMS by increasing the size of the error bars used. Figure 7 shows how different values of tau give different RMS errors. It was computed using 50 iterations on site MB08. The point at which the graph 'bottoms out' was used to determine what was a good tau value to settle on. In this survey a final tau of 10 was used for the 2D inversion process.

As stated previously, a smoother model containing reliable structures and constraints is preferable to a less smooth model that contains unrealistic structures and is unconstrained. The Tear function present on WinGLink allows the user to add constraints or 'breaks' to the model during inversion. For example, if it is known that there is basement contact at 2000m, a tear placed at 2000m will allow the inversion to consign a boundary at that depth rather than just smoothing over it. Tears allow us to add known structures and features to a model, or to test how theorised structures hold up against the data.

WinGLink offers the choice of standard grid or uniform Laplacian grid regularization. The uniform grid Laplacian operator resulted in a smoother model and was used for this purpose when performing the inversion. The regularization order used was |grad(m)|**2 as it gave better results during inversions. A horizontal weighting factor of 0.5 was used (1.0 being default with no weighting). The purpose of this was to attempt to minimise draping of the resistivity around the sites.

Results:

The models and results that were computed were based around 2 lines. The first and most important is the north south line. This is because of the orientation. It runs across strike of the regional geology and therefore shows more structure, it also contains MB1 which was taken over Beresford Spring itself. The second line runs east west and roughly follows the Oodnadatta Track. This line did not contain a site over a spring but still offers information about regional structure. Figure 8 shows the location of these lines, relative to the sites and to one another, as well as the survey sites location relative to the cross-section in figure 4. The site MB1 is of importance as it was taken over the spring itself. The purpose of this was to enable comparison of the spring outlet with sites some distance from the spring.

Figures 11-16 show the main results from the survey. Overall they show that there is no significant anomaly located beneath Beresford Spring that could represent fluid pathways feeding the spring. The inability to delineate these pathways suggests that flow is locally constrained and was not able to be detected by the survey. The spring itself was shown to be resistive in nature and is easily distinguishable from the surrounding geology.

Discussion:

Pseudo-sections

The pseudo-sections shown in figure 10 are slices at 100Hz, 10Hz, 1 second, 10 seconds and 30 seconds and are displayed in increasing depth. They show an overall trend of increasing

resistivity with depth, ranging from an average of just below 1 ohm meter at 100Hz to between 100-200 ohm meters at 30 seconds. This increase in resistivity is consistent with theory that states that resistivity will increase with depth (Simpson & Bahr 2005). Resistivity is largely dependent on porosity and water content, all of which decrease with an increase in pressure (Unsworth *et al.* 2007). This is consistent with what is shown in the sections, which on average become more resistive with depth. Beresford Spring (MB1) is consistently more resistive than the surrounding area on all of the slices. It is on an average a factor of 10 times more resistive then the surrounding confining beds. This increase in resistivity is likely a result of the flow of fresh water from the spring or a clogging of pore space due to the precipitation of carbonates. It is interesting to note that at MB11, there is a similar tenfold increase in resistivity compared to the surrounding area. There is no known spring at this location. MB11 stays more resistive than sites in the vicinity with increasing depth, similar to MB1.

Figure 16 is a pseudo section of the north south line with depth measured in seconds. There is a marked increase in apparent resistivity below MB1 at the spring. This is likely due to the flow of relatively fresh water through the spring. The apparent resistivity gradually rises from the north towards the spring, than sharply drops off again towards the south.

Phase Tensor

Phase Tensors are a way of representing the phase relationship in the form on an ellipse. These ellipses allow for easy representation of the direction of dominant conductivity and the level of skew, while still being independent of galvanic distortion (Caldwell *et al.* 2004). The major axis of the ellipse shows the direction of dominant conductivity, or the preferential direction of flow. The plots in Figure 12 show that below 1Hz, all the sites have an elliptical tensor that has its principal axis in a northeast southwest direction. This means that at depth, the entire region has a similar orientation of preferred electrical conductivity. As we get to shallower depths, the ellipses begin to lose their heterogeneity and there is no preferred orientation for electrical conductivity. Beresford Spring (MB1) is unique in this aspect; it maintains an ellipse with its principal axis in a northeast southwest orientation while all other sites do not. This tells is that the preferential direction of conductivity is in a northeast south west orientation. At 187.5Hz, Beresford (MB1) has virtually lost all heterogeneity and looks no different to the other sites.

Magnetotelluric Soundings

MT soundings show the raw data that is used to generate pseudo sections or what is used for the inversion process. Figure 13 shows the MT response of the sites for MB1 (Beresford Spring) and MB13. The purpose of these plots is to show the difference between the responses of Beresford Spring and the surrounding confining beds away from the spring. Through causal inspection, it is evident that there is at least a fivefold increase in apparent resistivity between the two sites. It was predicted that Beresford Spring would be a more resistive site. Moving away from MB1, the apparent resistivity decreases to responses more similar to MB13. There is noise present between 0.25 and 0.05Hz that was muted for the purpose of the 2D inversion but was left unmodified for this comparison. From 25Hz to 250Hz, The slope of the apparent resistivity for MB13 decreases to almost zero while there is almost no discernable change in slope for MB1 at this frequency range. For frequencies less than 0.25Hz, the slopes of the apparent resistivity's for both MB1 and MB13 decrease to zero while still maintaining a fivefold difference in resistivity. The phases are largely similar between the sites however there is some divergence at frequencies greater then 10Hz with MB1 having a smaller phase angle then MB13.

2D Inversion Models

Inversions integrate the data collected from multiple stations into a single model point. This gives a much more reliable and accurate representation then a pseudo section for example as the inverted data has been referenced by more than one source. Figure 14 is a 2D inversion model of the north south line shown in Figure 8. Figures 14.1 and 14.2 are the same model but have a different vertical scale. The draping that occurs past the furthest extents of the site locations is not accurate or reliable structure and is a remanent of the 2D inversion process. For approximately the first 200 meters, the Beresford Spring locality has a high conductivity ranging from 1-40 Ohm meters. This varies from site to site. Between MB4 and MB6 for example this zone of high conductivity only lasts for 50 meters, where as between MB18 and MB5 this zone extends down to 200 meters. This highly conductive zone is due to several reasons, primarily because at shallow depths there is low pressure, which allows for a high porosity. These pores contain water and salts which are highly conductive (Unsworth *et al.* 2007). Overburden present on the surface also tends to be conductive (this is due to higher porosity and water content), which would contribute. At depths there is high pressure, the pressure results in a low porosity, it forces cracks and fractures closed and results in there being very little fluids that would increase the conductivity (Kelly & Frohlich 1985). Between MB1 and MB4 there is a large increase in the resistivity gradient, almost a hundredfold increase over the space of a hundred or so meters. This is due a large resistive anomaly that exists beneath MB4 and MB6 which is two or three times more resistive then at similar depths at other sites. Looking at figure 14.2, there is a small anomaly that exists immediately below the surface at Beresford (MB1) within the top 20 meters. The resistivity increases from values below 10 ohm meters to above 50 quite abruptly then drops back down to below 10 ohm meters again. This is consistent with the spring being more resistive then the surrounding area due to movement of fresh water. It could also be a result of the clogging of pore space due to the precipitation of carbonates from the rising artesian water. A decrease in porosity results in an increase in resistivity. The response from Beresford is also consistent with a TEM survey that was performed by Flinders University (Berens 2010)**.** The TEM survey shows that the spring is more resistive than the surrounding geology, which is validated by the results of this study. The anomaly forms a tail that tapers off to the north towards MB7. If further constraint was applied in the form of another site just north of MB1, it is likely that this tail would disappear and the anomaly would be more consistent with the TEM survey.

Figure 15 is a 2D inversion model of the east west line shown in Figure 8. Figures 15.1 and 15.2 are the same model but have a different vertical scale. The model is very homogeneous and there is nothing immediately that stands out about it. There is a zone of high conductivity (1-10 ohm meters) to a depth of about 200 meters for the reasons described for Figure 14. Below that is the resistive zone that ranges from 50-100 ohm meters with no significant anomalies like in Figure 14. The cross-section in Figure 4 shows that the Bulldog Shale dips approximately 30 degrees to the north east. Closer inspection of Figure 15.2 reveals that there is a gentle slope to the conductive layer down in a north east direction at approximately 15 degrees. This is consistent with the Bulldog Shale that is shown in Figure 4 (there is horizontal exaggeration due to the horizontal extent of Figure 4 being approximately 50km while for Figure 14 it is 5km). The Bulldog Shale is conductive due to salty water trapped within the fine grained rocks.

There are several possible suggestions for further study, which still remain ambiguous despite current research. The possible influence of mantle derived fluids that feed into the spring may explain the source of the high He^4 present in the aquifer. This largely remains an unknown. There is the possibility of localised rainfall and infiltration from the tail of the spring feeding back into the aquifer. If this occurs, the extent at which it does is unknown. The springs occur as points along structurally controlling faults which raises the question as to why seepage from the

aquifer does not occur along the length of the fault. This indicates that there must be some preferential flow along the length of the fault.

Conclusion:

Beresford Spring is identified by a zone of increased resistivity surrounded by zone of low resistivity. The pseudo-sections in Figure 11 all show a marked (five to tenfold) increase in resistivity at the spring (MB1) which is surrounded more conductive geology. This is further corroborated by comparison of the MT soundings from MB1 and MB13 which show a distinct change in resistivity and a divergence in slopes for frequencies >10Hz. While there were some similarities between MB1 and MB11 in the pseudo-sections, this was not substantiated any further by subsequent results. There is a small zone of increased resistivity directly below the spring (MB1) that can be seen in Figure 14 which can also be seen in the pseudo section shown in Figure 16. This is due to the flow of fresh artesian water from the aquifer. The surrounding confining beds (see Figure 3) consist of tight, fine grained rocks that contain trapped saline water, resulting in the more conductive zone surrounding the spring. This is substantiated by Figure 13 which shows the raw MT soundings of MB1 and MB13, making apparent the differences in resistivity. The slope of the conductive layer present in Figure 15 is consistent with the slope of the Bulldog Shale present in Figure 4. This constraint allows us to have an increased confidence in the accuracy of the model as a whole.

The phase tensor plots shown in Figure 12 reveal that at depth, there is homogeneity across the survey site with the direction of dominant conductivity in a NE-SW orientation. Where Beresford Spring becomes unique is at shallower depths, where it maintains this dominant conductivity orientation all the other sites lose any preference for dominant orientation. The spring being more resistive could allow shorter periods to penetrate deeper, which would result in the same series of fractures to be seen at shorter periods.

From the data collected, our main conclusions are that there is not strong evidence showing significant fluid paths. This does not preclude there being fracture paths, only that they have not been resolved. The fact that there is no major anomaly over a broad area beneath the spring suggests that flow is quite locally constrained. It is possible to detect the difference in apparent resistivity between the springs and the surrounding confining geology. The resistive nature of the springs may be due to two reasons. The first is the presence of fresher, flowing water exiting the spring compared to the surrounding geology which contains saltier, more confined water. The second reason is a reduction in porosity around the spring outlet, this is due to the clogging of pore space. This clogging would be a result of the precipitation of carbonates from the artesian water. The data also suggest that the basement geology is largely resistive. This is likely a result of the increased pressure at depth forcing closed fractures and pores restricting any fluid flow and the resulting mineralogy that is stable at these depths and temperatures. It could also indicate that the basement is anisotropic, with the orientation of smaller faults aligning in a north-east south-west orientation. The MT data does not delineate anything significant however we are confident that more data and possibly 3D coverage over the spring would allow for the resolution of the fluid pathways.

References:

ALNRMB 2008. *The Oodnadatt a Track - String of Springs. Government of South Australia*. Natural S. A. A. L. & Board R. M. **1:** 12. Government of South Australia, Adelaide.

BERENS V. 2010. *Beresford Spring Cross-section. PDF*. x-section. Flinders University, Adelaide.

BOX J. B., DUGUID A., READ R. E., KIMBER R. G., KNAPTON A., DAVIS J. & BOWLAND A. E. 2008. Central Australian waterbodies: The importance of permanence in a desert landscape. *Journal of Arid Landscapes* **72**, 1395-1415.

CALDWELL T. G., BIBBY H. M. & BROWN C. 2004. The Magnetotelluric Phase Tensor. *Geophysics* **158**, 457-469.

CHAVE A. D. & THOMSON D. J. 2004. A bounded influence regression estimator based on the statistics of the hat matrix. *Applied Statistics* **52**, 307-322.

HABERMEHL M. A. 1980. The Great Artesian Basin. *Australian Journal of Geology and Geophysics* **5**, 9-38.

KELLY W. E. & FROHLICH R. K. 1985. Relations between aquifer electrical and hydraulic properties. *Groundwater* **23**, 182-189.

KEPPEL M. 2009. Mound Spring Carbonates - A window into the Palaeohydrologyof GAB Mound Springs.

KRESS W. H. & TEEPLE A. P. 2003. Two-Dimensional Resistivity Investigation of the North Cavalacade Street Site, Huston, Texas, August 2003. *USGS Scientific Investigations Report 2005-5205*.

LOVE A. & HERCZEG A. 2007. Review of Recharge Mechanisms for the Great Artesian Basin. *CSIRO*.

LOVE A., HERCZEG A., SAMPSON L., CRESSWELL R. G. & FIFIELD L. K. 2000. Sources of chloride and implications for Cl36 dating of old groundwater, south-western Great Artesian Basin, Australia. *Water Resources* **36**, 1561-1574.

MUDD G. M. 2000. Mound springs of the Great Artesian Basin in South Australia: a case study from Olympic Dam. *Environmental Geology* **39**, 463-476.

NRM Q. 2006. The Great Artesian Basin. *Natural Resources and Water* **1**, 1-2.

RODIE W. & MACKIE R. L. 2001. Nonlinear conjugate gradients algorithm for 2-D magnetotelluric inversion. *Geophysics* **66**, 174-187.

SIMPSON F. & BAHR K. 2005. *Practical Geophysics* (Vol. 1). Cambridge University Press, Cambridge.

TORGERSEN T. 1980. Controls on porefluid concentration of He4 and Rn222 and the calculation of He4/Rn222 ages. *Journal of Geochemical Exploration* **13**, 57-75.

TORGERSEN T. & CLARKE W. B. 1985. Helium accumulation in groundwater, an evaluation of sources and the continental flux of crustal He4 in the Great Artesian Basin, Australia. *Geochim Cosmochim Acta* **49**, 1211-1215.

TORGERSEN T., HABERMEHL M. A. & CLARKE W. B. 1992. Crustal helium fluxes and heat flow in the Great Artesian Basin, Australia. *Chemical Geology* **102**, 139-152.

UNSWORTH M., SOYER W., TUNCER V., WAGNER A. & BARNES D. 2007. Hydrogeologic assessment of the Amchitka Island
nuclear test site (Alaska) with magnetotellurics. *Geophysics* **72**, 47-57.

WILLIAMS A. F. & HOLMES J. W. 1978. <A novel method of estimating the discharge of water from mound springs of the Great Artesian Basin, central Australia.pdf>. *Journal of Hydrology* **38**, 263-272.

Figures:

Figure 1. The location of Beresford Spring relative to Lake Eyre and the Oodnadatta Track and inset, the map's location relative to the Great Artesian Basin.

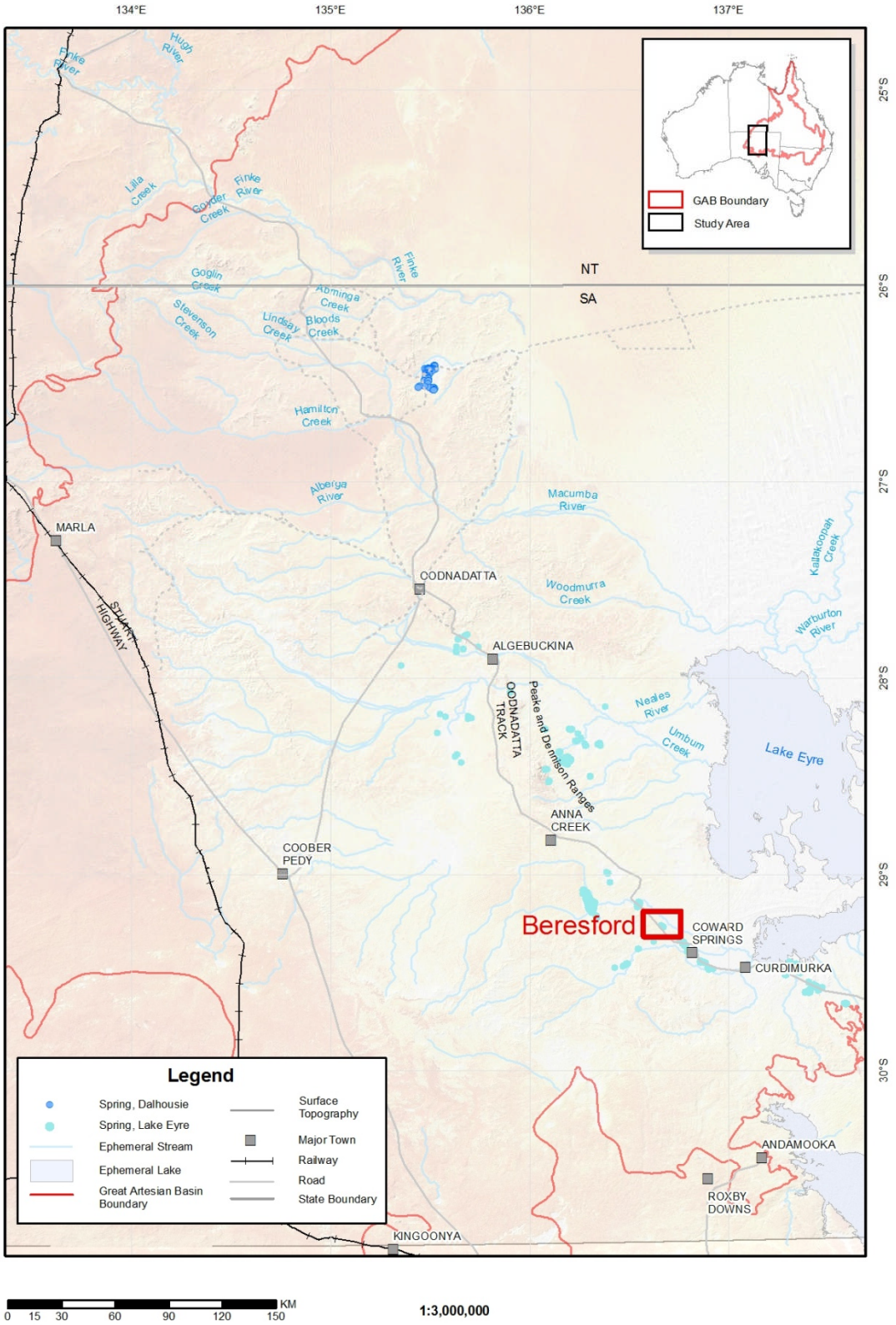

Figure 2. A schematic representation of an artesian basin showing a zone of initial infiltration and ex-filtration through a structurally controlled artesian spring. Source: University of Memphis.

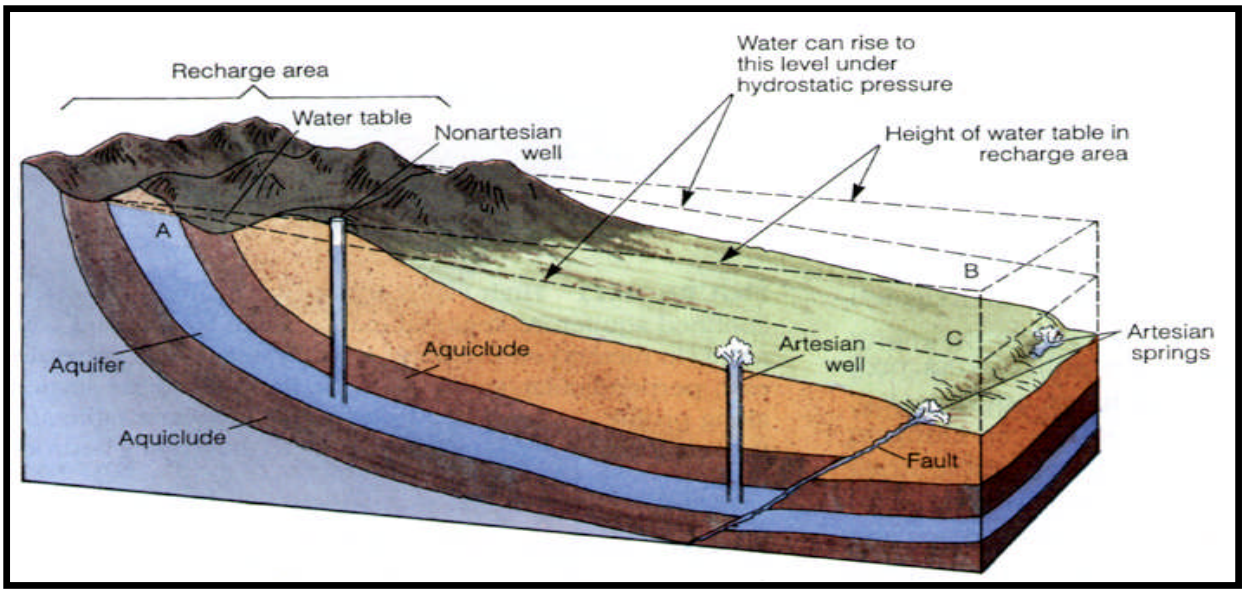

Figure 3. Schematic representation of a mound spring. Rising fluids are responsible for the accretion of sediments around the spring outlets eventually building up to form a mound (Williams & Holmes 1978) (Mudd 2000)

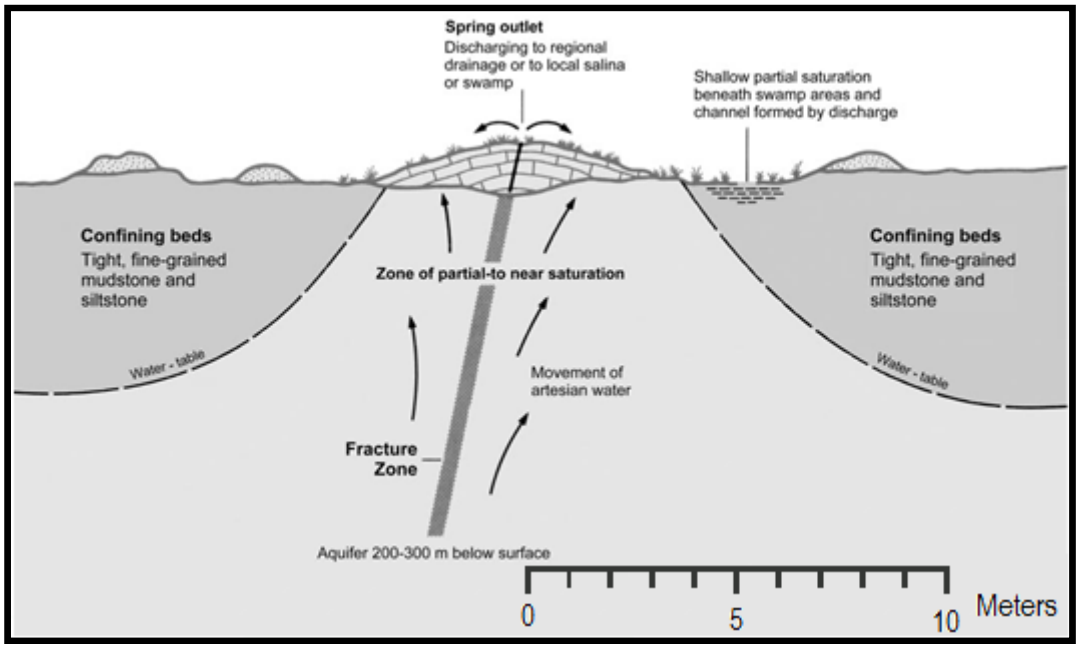

Figure 4. A geological cross-section of the greater Beresford Spring region. The annotation represents the lateral extent of figure 15 relative to the cross-section. The formations dip to the north east at approximately 30 degrees and are intersected by a series of poorly constrained faults (Keppel 2009)

Figure 15

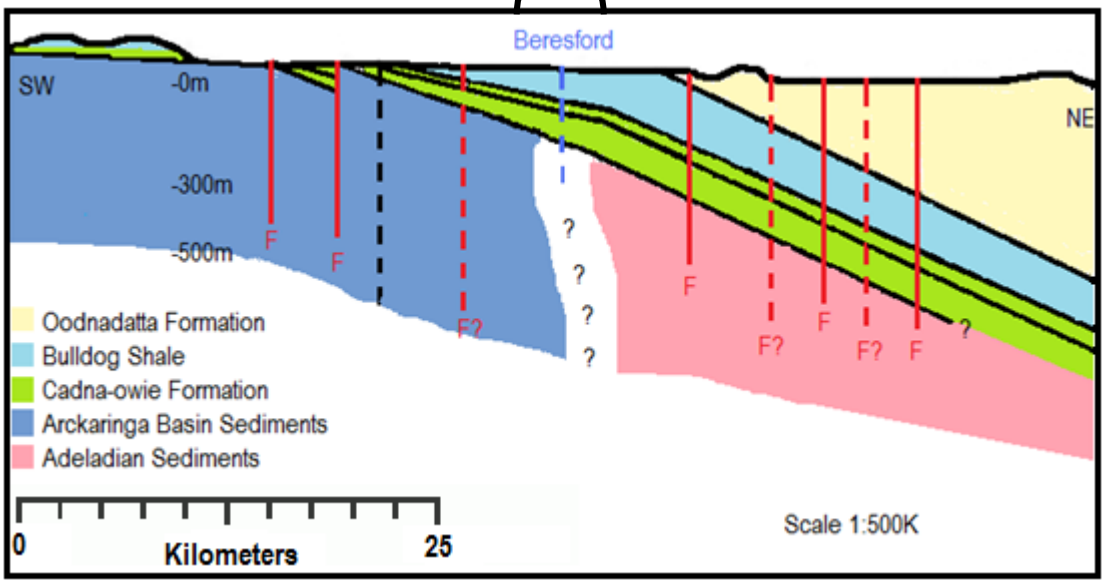

Figure 5. A representation showing how a transmitter (in the case of MT, variations in the Earth's magnetic field) induces currents within a conductor that can be detected via magnetometers and electrodes. Source: (Simpson & Bahr 2005)

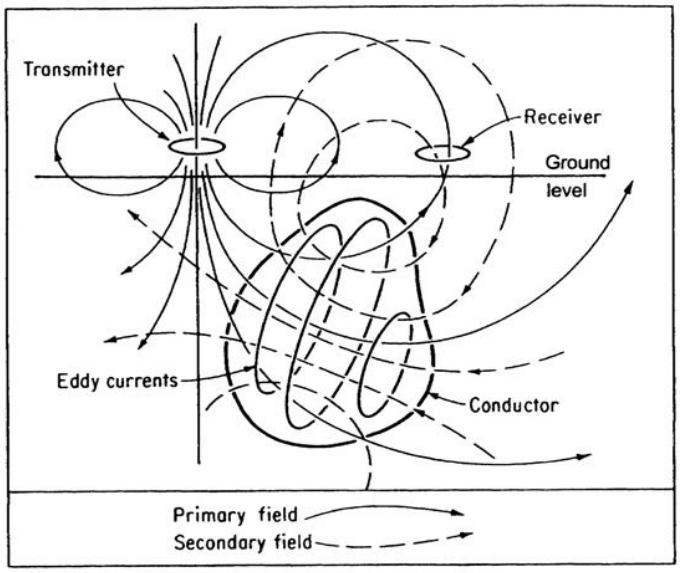

Figure 6. An example of raw time series data from the site MB11. The large blue spikes in the magnetic field B are the result of fluctuations caused by electrical storms, specifically lightning. Each spike in the B field is matched by a lower intensity spike in the electric field E. This relationship between B and E is explained by Maxwell's equations.

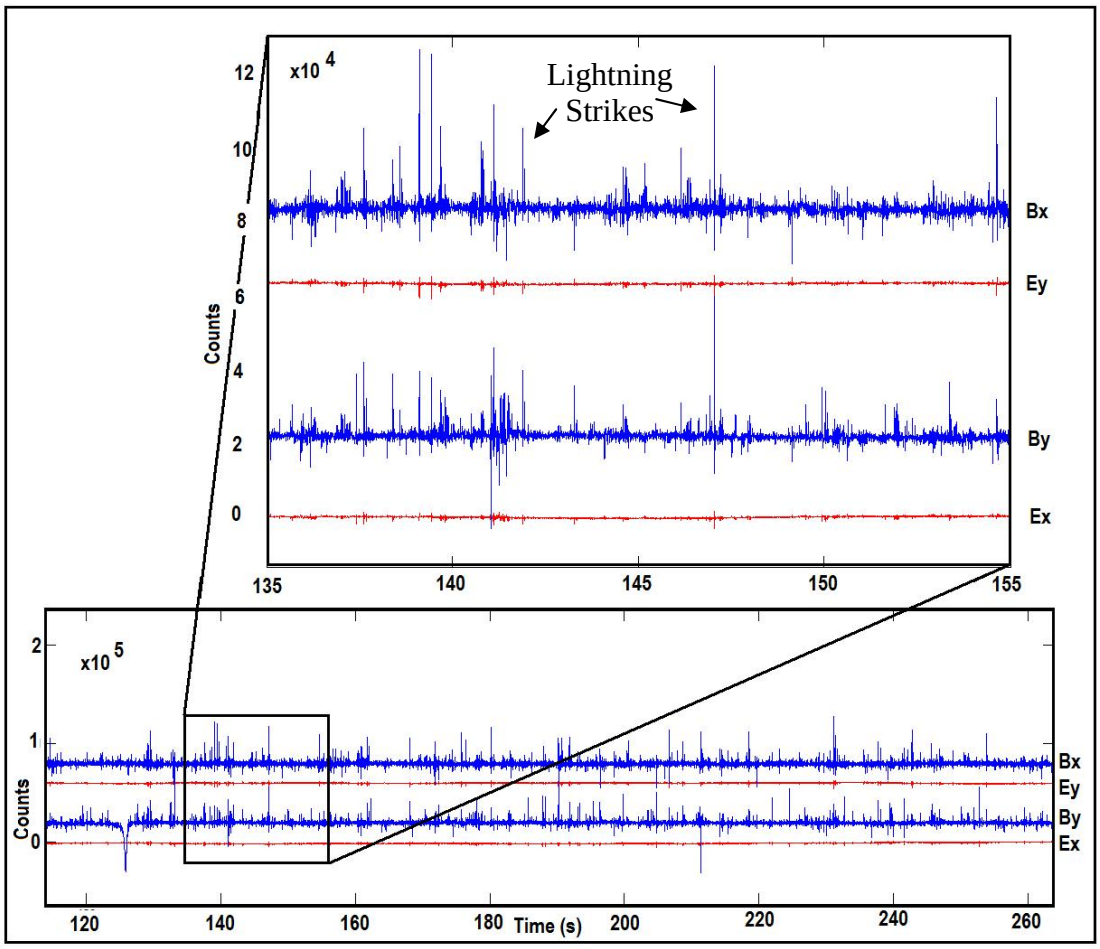

Figure 7. A table showing the resultant RMS error values for differing the smoothing factor Tau. Below is a graph of the data that was used to determine the optimal value for Tau, in this case 10. This is the point at which lowering Tau further begins to have a smaller impact on the RMS error.

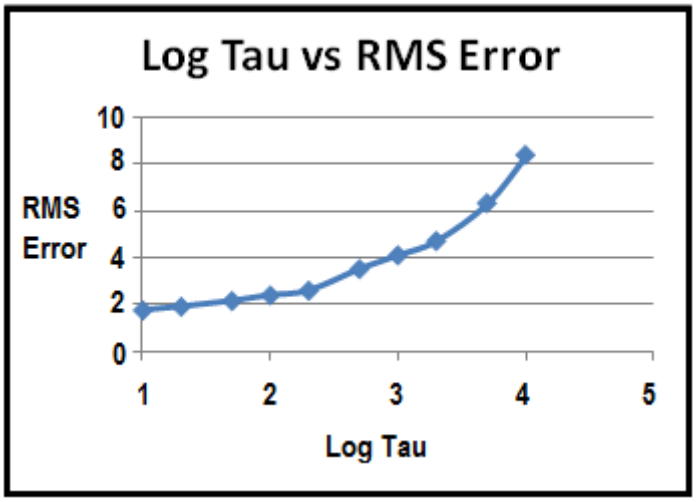

Figure 8. Locations of the MT deployments and position of the 2D Inversion lines. The purple line represents the extent of the cross-section (Figure 4) and inset, a satellite image showing the positions of Beresford and Warburton Springs with the proximate MT sites.

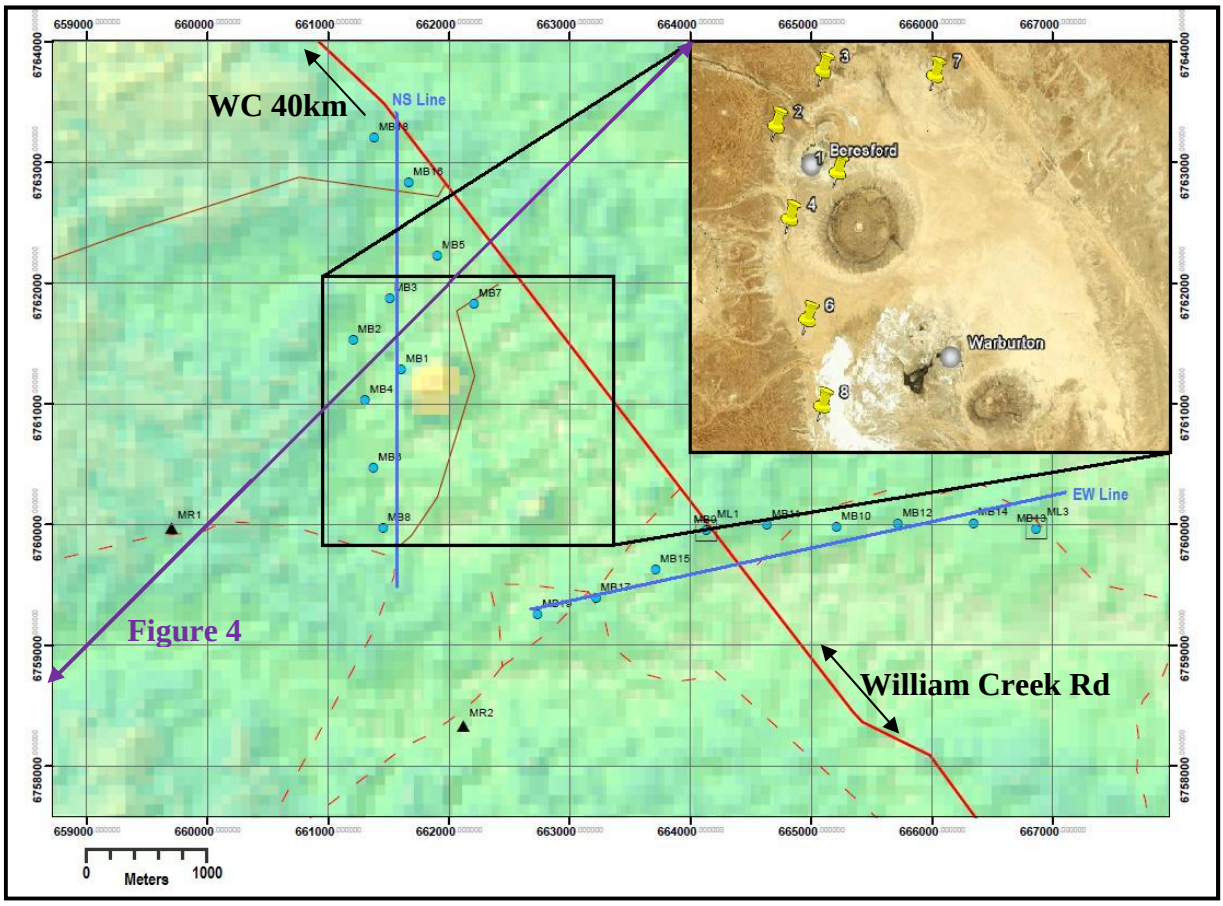

Figure 9. This image shows Apparent Resistivity vs. Frequency for the site MB10. The first is pre-processing (figure 9.1). The second is post-processing (figure 9.2). The red arrow indicates a drop in coherence due to noise. This drop is removed via coherence thresholding and remote referencing and the improvement shown in 9.2.

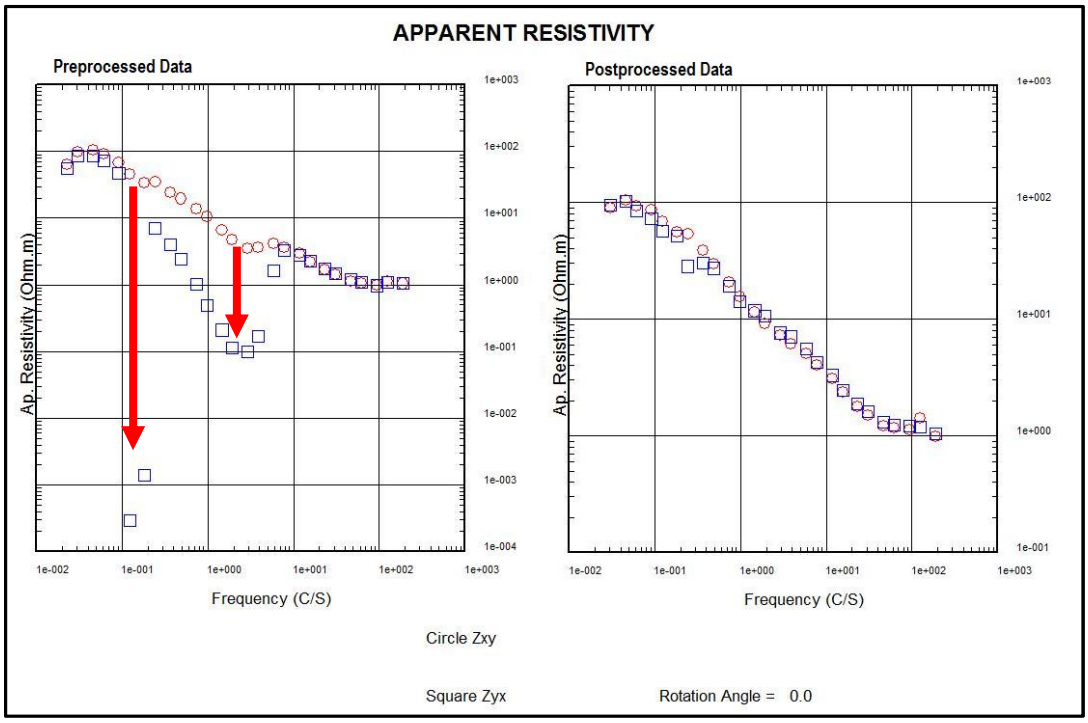

Figure 10. TEM survey of Beresford Spring. The spring, more resistive is surrounded by more conductive confining layers. The spring is identified by the arrow. Source: (Berens 2010)

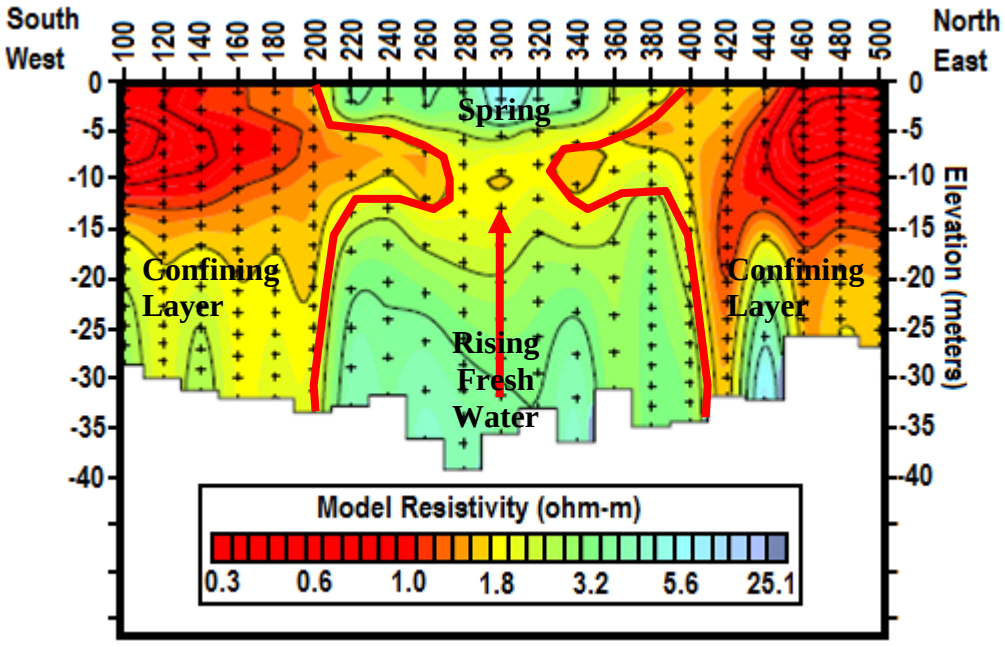

Figure 11. These Pseudo Sections show a general increase in resistivity with increased depth with an anomaly at Beresford Spring (MB1). This difference is due to the flow of relatively fresh water from the spring compared to salty water trapped within the surrounding confining layers.

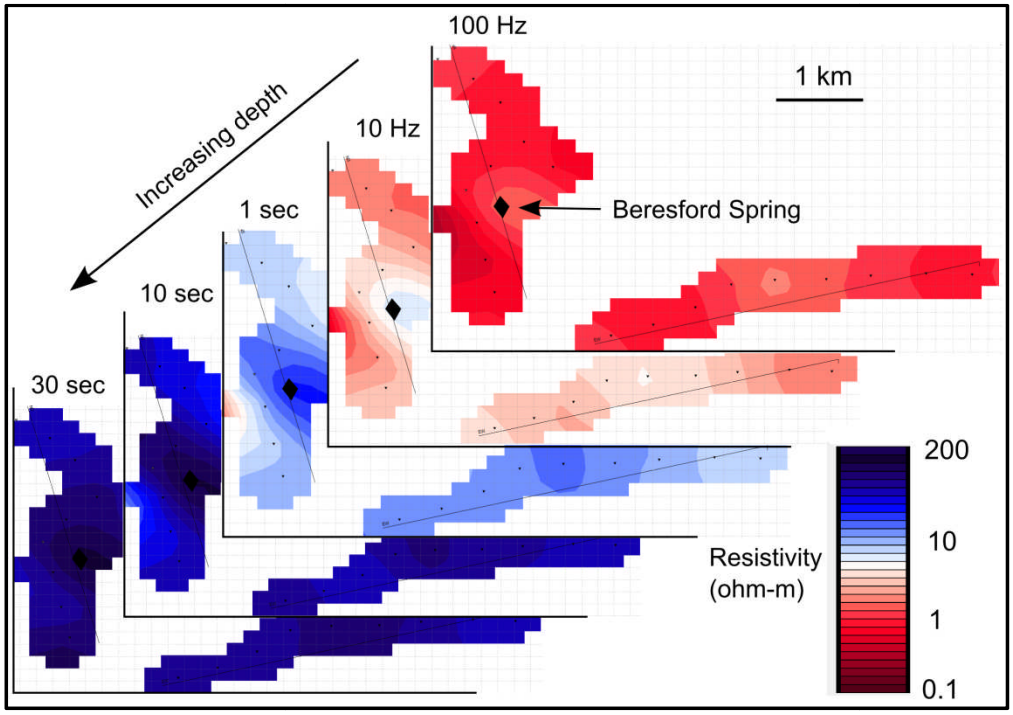

Figure 12. Plots of Phase Tensors showing Beresford spring with a NE-SW orientation that differs from all the other sites. At deeper depths the sites become homogeneous and indistinguishable from the spring.

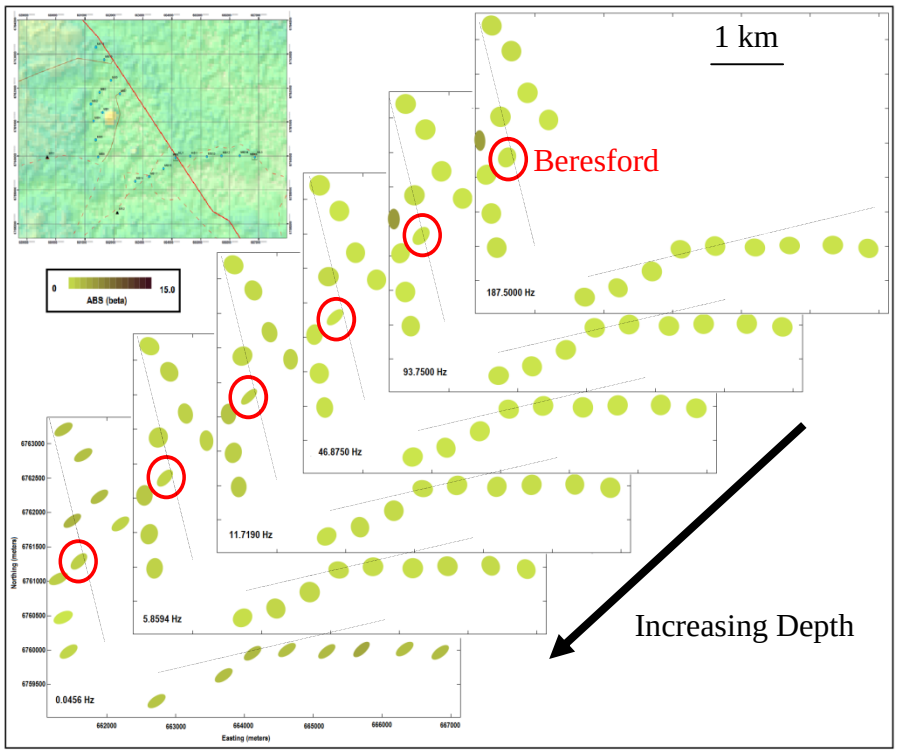

Figure 13. Apparent Resistivity and Phase vs. Frequency plots comparing the responses for MB1 (Beresford Spring) and MB13. The purpose of this is to show the difference between the response of the spring and areas away from the spring.

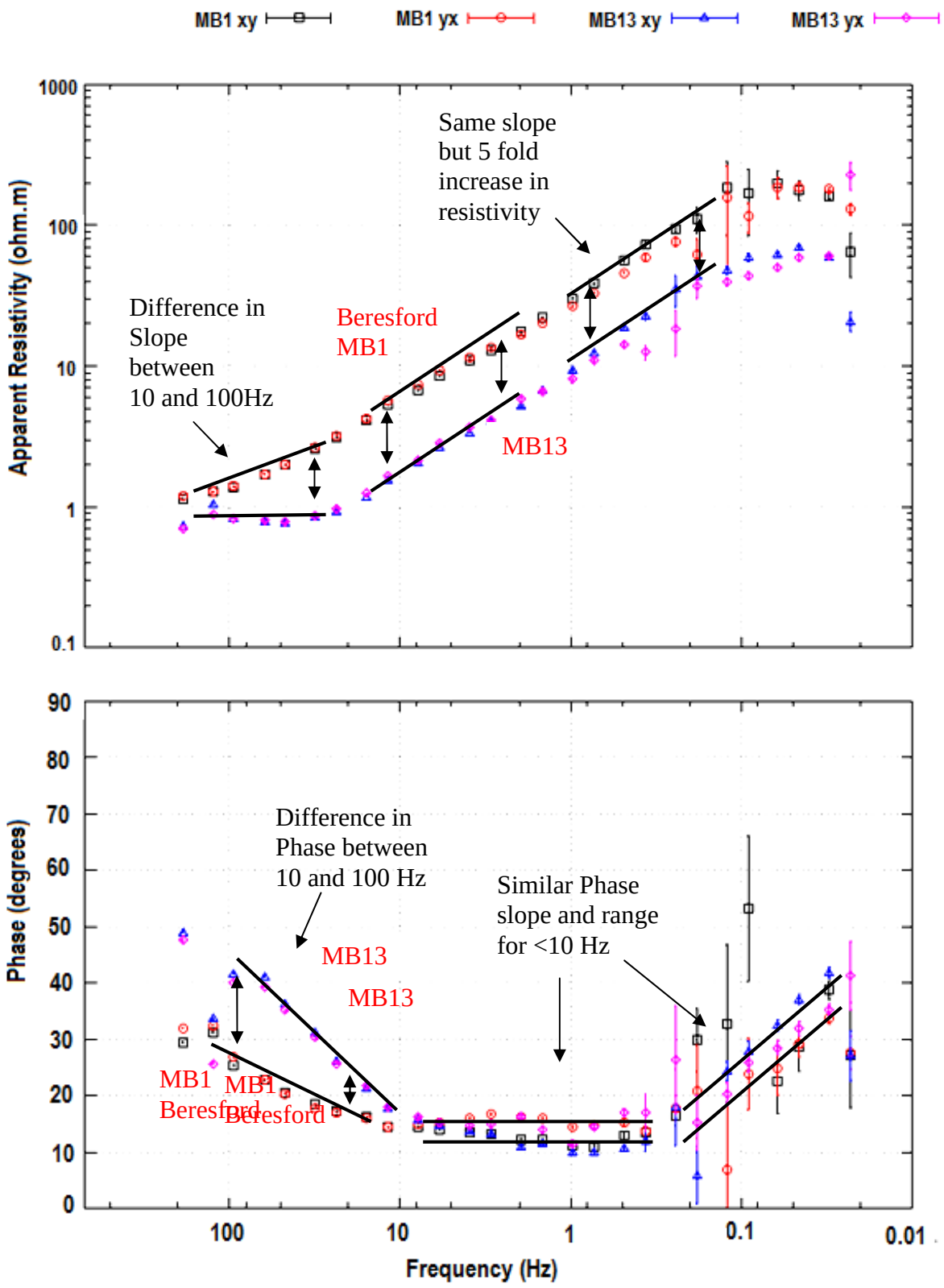

Figure 14. 2D Inversion model of the NS line depicted in figure 8, the first (figure 14.1) down to 5000m and the second (figure 14.2) to 500m depth. Figure 14.2 has an inset of the TEM survey shown in figure 10 which corroborates the inversion.

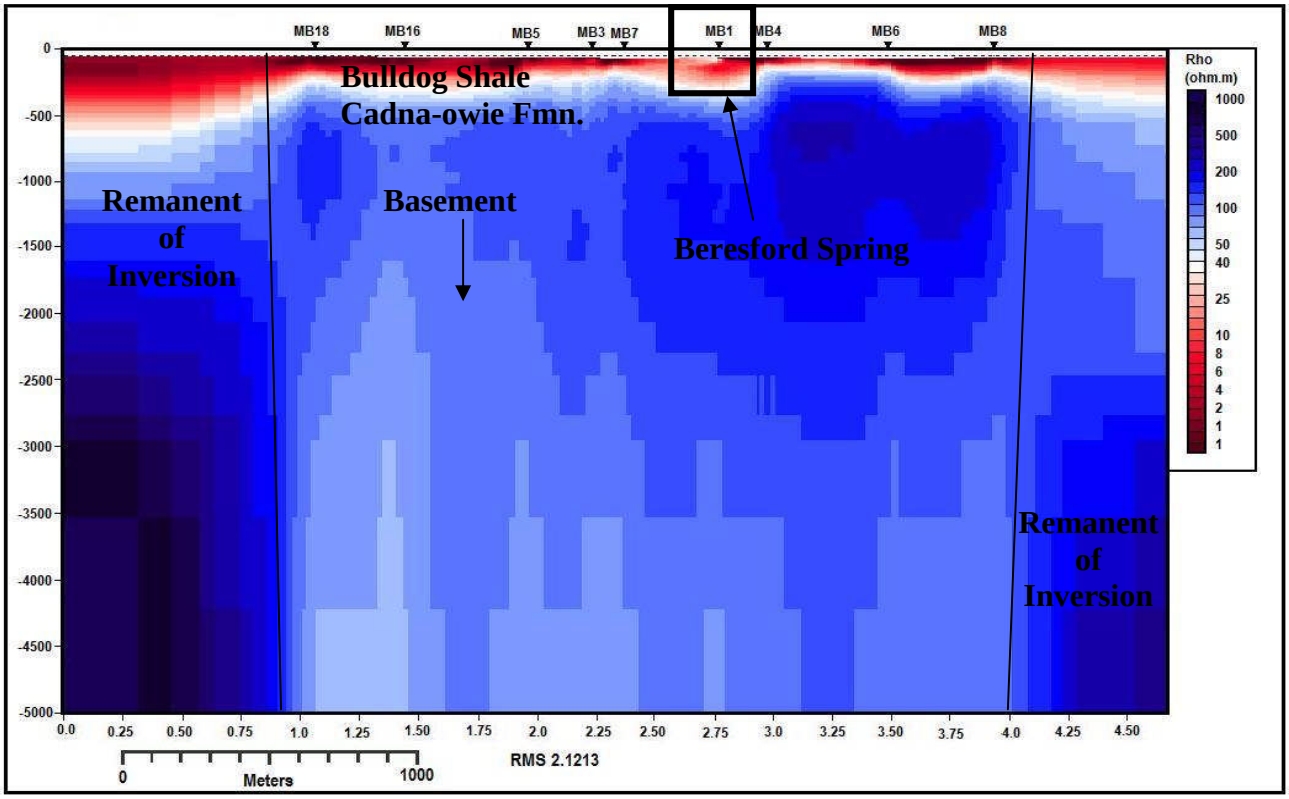

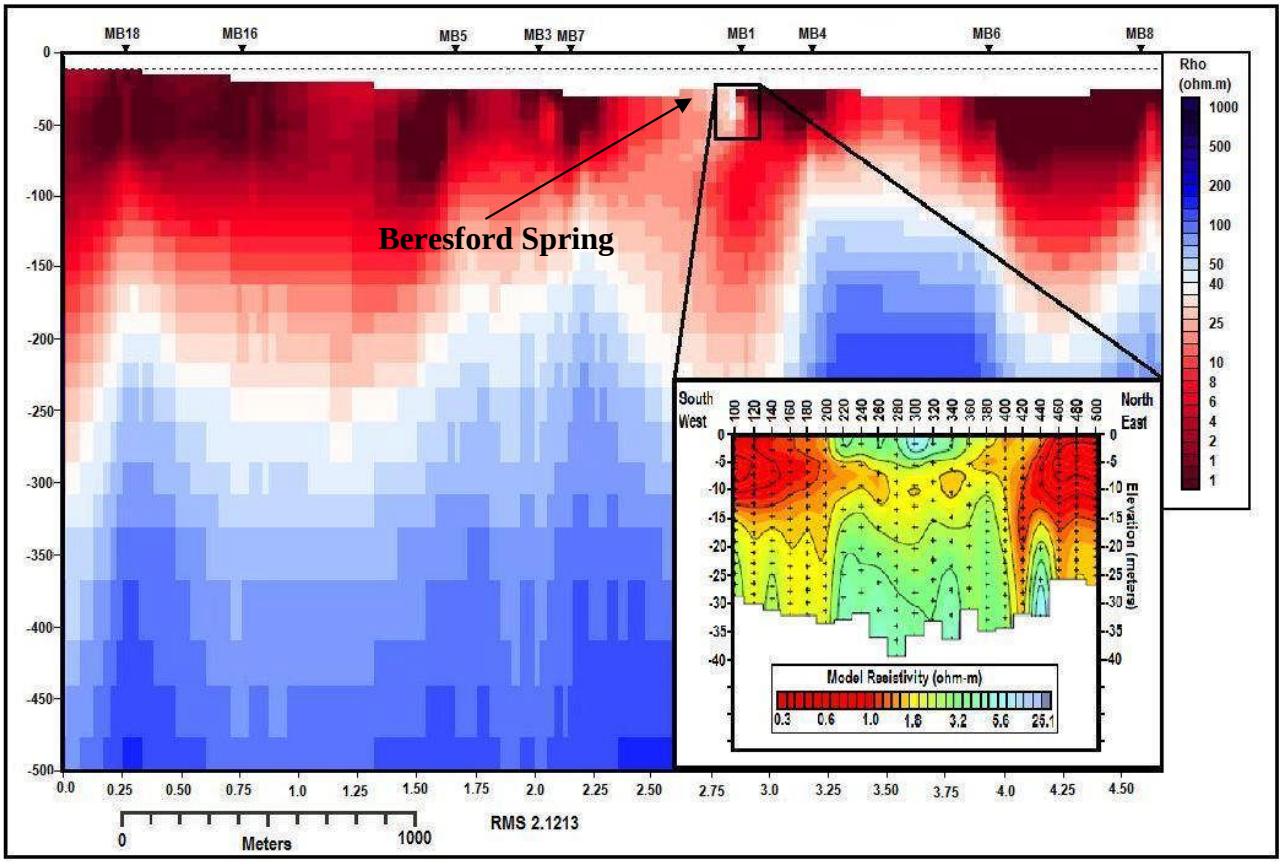

Figure 15. 2D Inversion model of the EW line depicted in figure 8, the first (figure 15.1) down to 5000m and the second (figure 15.2) to 500m depth. They show that there is a gradual slope in resistivity towards the west which is supports the cross-section shown in figure 4.

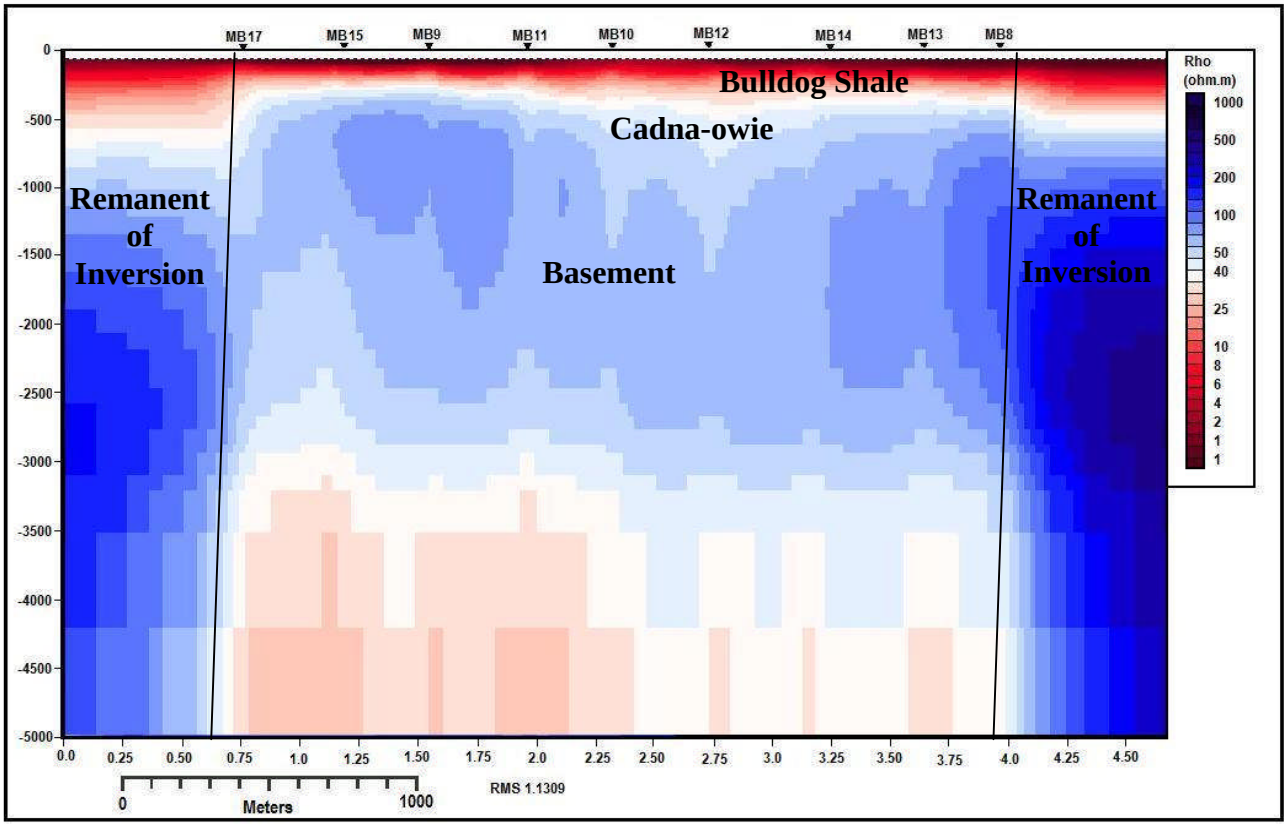

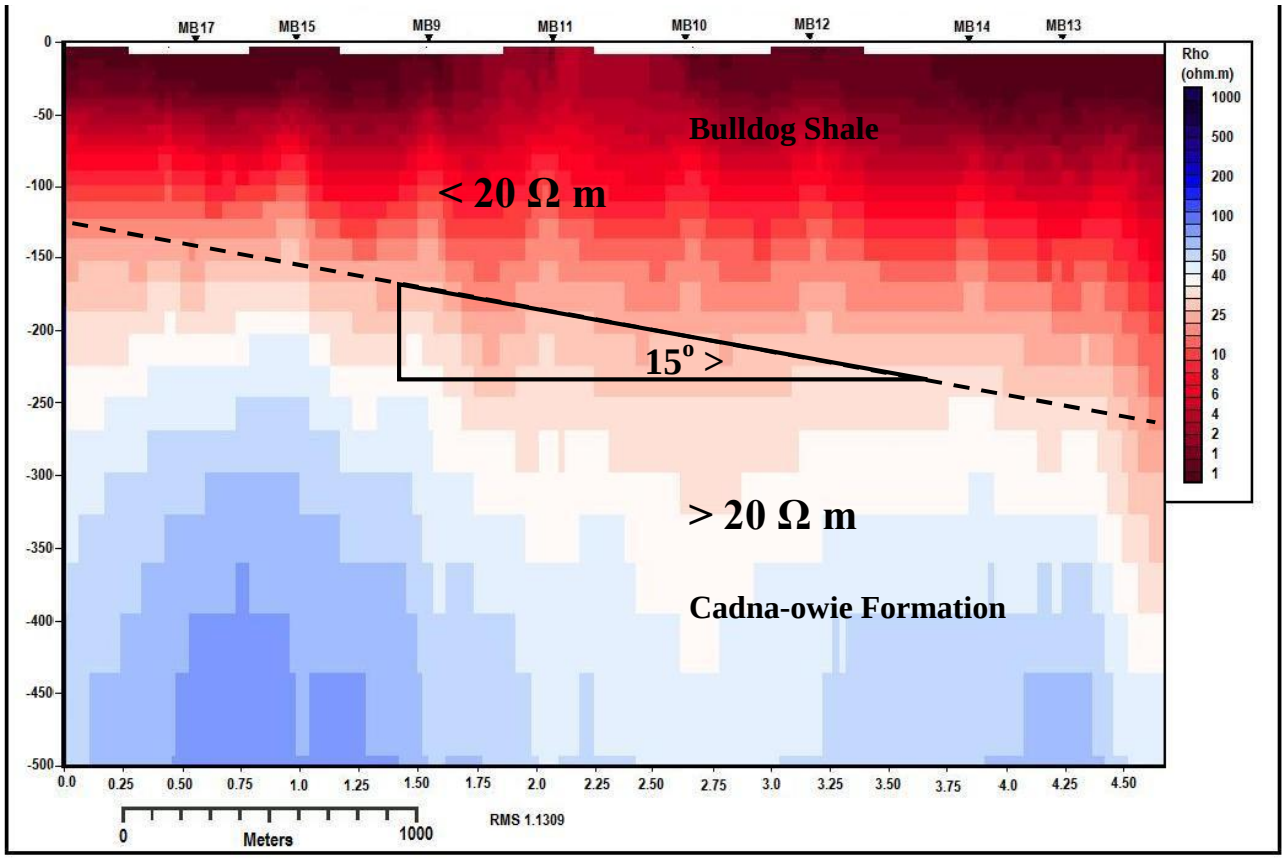

Figure 16. Pseudo Section of the north south line depicted in figure 8. There is a marked increase in apparent resistivity below MB1 at the spring. This is likely due to the flow of relatively fresh water through the spring.